A STUDY OF QUASI-STATIC DELAMINATION IN SANDWICH STRUCTURES

Srinivasan Sridharan and Yupeng Li
Washington University in St. Louis, St. Louis, Missouri, 63130, USA
E-mail: ssrid@seas.wustl.edu

Abstract
Delamination of sandwich columns is studied using a relatively simple cohesive layer model. The model is described in some detail and is incorporated as a user supplied element (UEL) in a finite element package. The model is shown to predict accurately the test results of delamination of a facing sheet of a sandwich member. The accuracy of the model is seen to be superior to a model previously proposed by the authors, which predicts an earlier termination of crack growth. The UEL model is applied to a sandwich column investigated by earlier investigators – a column that is relatively stout (ratio of length (L) to depth (d) ≈ 7.3) and has stiff facing sheets (ratio of depth d to the thickness (h) of facings ≈ 15). The model is able to capture the onset of delamination buckling, sudden delamination growth at nearly constant compression, stable delamination growth and reaching of a limit point of the load carrying capacity. A slender sandwich column with relatively thin facings (L/d ≈ 15, d/h ≈ 40) is next considered. It indicates that overall bending tends to inhibit delamination growth under quasi-static loading as it tends to keep the delaminated surfaces in contact.

Introduction

An often encountered failure mode of sandwich structural components is the core facing debonding. Once such debonding occurs the integrity of the structure is compromised and a significant reduction in the stiffness and the load carrying capacity occurs. A sandwich member under compression is delamination-sensitive as the delaminated skin tends to buckle thus accentuating the risk of delamination growth.

Under quasi-static loading the extent of the growth of delamination depends upon the overall bending stiffness of sandwich beam as a whole as well as the bending stiffness of the delaminating facing sheet. As the structure bends in an overall sense, delamination tends to close notwithstanding the sense of bending and inhibit the growth of crack. The delamination growth may come to a standstill despite a continuing increase in the load carried. By the same token the delamination growth is inhibited in a sandwich column undergoing wrinkling - a mode of deformation composed of short waves. (The last point, however, is of academic interest only, as with the onset of wrinkling the total exhaustion of the load carrying capacity is not far.)

Previous experience (Sridharan, S., 2001 and El-Sayed, S. et al, 2002) has indicated that the delamination failure in sandwich members is principally in mode I (opening mode) with shear playing a negligibly small role. Thus the most significant parameter required for tracing the delamination growth is the critical value of strain energy release rate (SERR), viz. G_{Ic}. In order to trace the delamination growth without interference by the user, a cohesive layer model interposed between the facing and the core is employed. Authors have developed two types of the model (Li, Y. et al, 2005) which are used in conjunction with a widely used nonlinear finite element program (Abaqus, 2001):

(i) UMAT model: The cohesive layer is of finite thickness and represented by a layer of elements of a type available in a standard finite element package, but with *user supplied material* properties, hence called the UMAT model. The material property that is significant here is the relationship between incremental stress and incremental strain in the transverse direction.

(ii) UEL model: The cohesive layer has zero thickness initially and is represented by a set of *user supplied elements.* The user has to define the nodal forces and the current stiffness of the elements based on the relative displacement suffered by the element between its two separating surfaces.

M. Pandey et al. (eds), Advances in Engineering Structures, Mechanics & Construction, 615–626.

An effort is made to maintain utmost simplicity in the formulation of the model in either form. The paper also discusses briefly selection of the maximum cohesive stress of the material – which is crucial for capturing the crack initiation point precisely. It is seen, as in the case of laminated composites (Li, Y. et al, 2005) that the UMAT model ceases to be reliable as the crack advances and predicts a premature shutting down of crack growth.

Cohesive Layer Models

UMAT Model

This model employs a constitutive relationship in the form of a stress-strain relationship of the cohesive layer. The stresses and strains of the cohesive layer element are referred to axes which rotate with the element. Thus the effect of rigid body rotations is eliminated in the incremental strain-displacement relations. The model is defined in terms of the parameters describing the stress-strain relationships and the thickness of the cohesive layer. In the present context only the normal stress-strain relationship in the transverse direction is of pertinence, other relationships are assumed linear elastic. Poisson ratio is set to zero. For simplicity a nonlinear elastic relationship consisting of a linear elastic phase given by the modulus E_2 followed by a phase in which stress remains constant at σ_{max} (similar to "elastic-perfectly plastic" response) is assumed. The values of E_2 and σ_{max} must be representative of the core material through which the crack propagates. The other significant parameter is the thickness of the cohesive layer h_0, the initial thickness of the cohesive layer. Ideally h_0 is based on the observed dimensions of the process zone (Li, Y. et al, 2005). However the smallest possible dimension consistent with computational economy and reliability is chosen in the present work.

The cohesive material response calculations are performed in a module (UMAT) attached to the input program of Abaqus. A 4-noded plane strain/plane stress elements with reduced integration are selected for the cohesive layer for 2-D problems. Since reduced integration is used, a single integration point represents the whole element. The incremental strain ($\Delta\varepsilon_n$) is based on the current cohesive layer thickness h_c and so the total strain is approximately logarithmic[6]. As the nonlinear analysis proceeds, the value of G_I is monitored as in:

$$G_I = \sum \sigma_n h_c \Delta\varepsilon_n \tag{1}$$

Failure is deemed to occur as soon as the following fracture criterion is satisfied: $G_I \geq G_{Ic}$. The main program supplies the incremental strains which are based on the current (updated) dimensions and the user supplied material subroutine (UMAT) returns to the main program material stiffness matrix and the stresses at the integration point.

UEL Model

This cohesive layer model has zero initial thickness and is represented as a line in the undeformed state. Elements constituting the layer begin to acquire finite thicknesses as delamination occurs under mode I. The notion of strain is suspended and relative displacements of the nodes of the element are used to characterize the deformation and compute the nodal forces. Elements in model are 4-noded with 2 displacement degrees of freedom per node. The incremental deformation is characterized in terms of averaged normal relative displacement $\Delta\delta_1$ computed from the incremental nodal displacements. The stresses in the element are related to δ_1 and δ_2 respectively via nonlinear elastic relationships consisting of two phases (a linearly varying stress phase and a constant stress phase). δ_{10} and δ_{20} are the proportional limits of δ_1 and δ_2 and are prescribed taking into consideration of the stiffness of the material and the thickness of the process zone. They can be estimated as $\delta_{1o} \approx \frac{\sigma_{max}}{E_2} t$, $\delta_{2o} \approx \frac{\tau_{max}}{G_{12}} t$ where t represents process zone thickness; further δ_{10}, and δ_{20} must be chosen to be sufficiently small so that the elastic strain energy contribution is small compared to the cohesive strain energy in the layer. Nodal forces and the stiffness matrix are found in terms of the stress state in the

element. These are transformed to the global axes and returned to the main program. The total strain energy stored per unit area in each mode in the element is given as a sum of incremental contributions as follows:

$$G_{Ic} = \sum \sigma_n \Delta\delta_1 \tag{2}$$

Failure is deemed to occur as soon as the following fracture criterion is satisfied: $G_I \geq G_{Ic}$.

Fig. 1 shows a typical element ABCD and its deformed configuration A'B'C'D'; the original coordinates and displacements are given by (x,y) and (u,v) respectively with appropriate subscripts. The main program supplies for each increment of loading the current nodal displacements at the end of the previous loading increment and their corresponding increments for each iteration with reference to the global coordinate system.

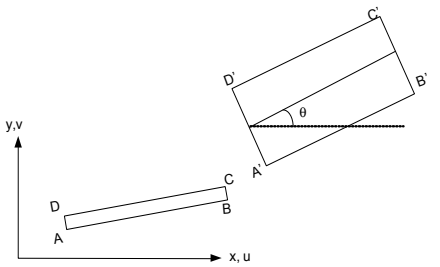

Fig. 1. Typical element ABCD and its deformed configuration A'B'C'D'

If θ is the averaged orientation of the element with reference to x-axis, then,

$$\tan(\theta) = \frac{y_2 - y_1}{x_2 - x_1} \tag{3}$$

Where:

$$\begin{aligned} y_2 &= \frac{(y_C + v_C) + (y_B + v_B)}{2}; \quad y_1 = \frac{(y_D + v_D) + (y_A + v_A)}{2} \\ x_2 &= \frac{(x_C + u_C) + (x_B + u_B)}{2}; \quad x_1 = \frac{(x_D + x_D) + (x_A + x_A)}{2} \end{aligned} \tag{4}$$

The current relative displacements in the normal (δ_1) and tangential directions (δ_2) with respect to the current orientation of the element are then computed by transformation:

$$\begin{aligned} \delta_1 &= (v_2 - v_1)\cos\theta - (u_2 - u_1)\sin\theta \\ \delta_2 &= (v_2 - v_1)\sin\theta + (u_2 - u_1)\cos\theta \end{aligned} \tag{5}$$

where:

$$\begin{aligned} u_1 &= \frac{u_A + u_B}{2}; \quad u_2 = \frac{u_C + u_D}{2} \\ v_1 &= \frac{v_A + v_B}{2}; \quad v_2 = \frac{v_C + v_D}{2} \end{aligned} \tag{6}$$

Note A coincides with D and B with C in the original configuration. From the assumed stress-displacement relations, the normal and shear stresses carried by the element are determined. These in turn are employed to determine the nodal forces in terms of the element length. The tangential stiffness matrix for the element is set up by appropriate differentiation. The current nodal forces and the tangential stiffness matrix are then transformed to the global axes and returned to the main program. Note that the nodal forces are updated for every iteration.

Calibration and evaluation of performance of the models using a test case

Li performed tests (Li, X. et al, 2000) on a sandwich member of length 210mm completely restrained at its top face and loaded uniformly across its width at one end of the bottom facing. The specimen carried a pre-implanted delamination of 51mm. The geometry, the loading and the boundary conditions of the test specimen are indicated in Fig. 2. Of the three groups of specimens tested, only one group identified as "KKV sandwich", exhibited no crack kinking into the core. After the first micro-kink, the crack propagated in the core parallel to the interface about 0.5mm below the face/core interface. The specimens were loaded at varying, but small angles to the normal of the top face and the one loaded normal to face is selected for investigation here.

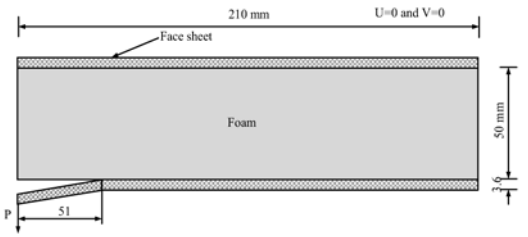

Fig. 2. Test configuration of Li's sandwich specimen

The facing sheets are made up of E-glass/vinyl ester while the core material is H200 Divinycell PVC foam. Table 1 lists the elastic properties of the materials. Here we use the averaged elastic properties as determined from compression and tension tests. (The most important property is the effective modulus in the longitudinal direction which determines the slope of the initial linear phase prior to crack initiation which varied from 23.2GPa in compression to 26.0GPa in tension - an average value of 24.6GPa is used for the comparison with experiment.).

Table 1: Material properties of Li's specimen

Material Property	Li's specimen	
	Face sheet	Core
Longitudinal Young's modulus, E_x (GPa)	24.6	0.165
Transverse Young's modulus, E_y (GPa)	11.8	0.263
Out-of-plane Young's modulus, E_z (GPa)	13.5	0.165
Poisson's ratio, υ_{xy}	0.31	0.32
Poisson's ratio, υ_{xz}	0.533	0.32
Poisson's ratio, υ_{yz}	0.446	0.32
In-plane shear modulus, G_{xy} (GPa)	3.78	0.0644
In-plane shear modulus, G_{xz} (GPa)	9.19	0.0644
In-plane shear modulus, G_{yz} (GPa)	3.74	0.0644
Critical strain energy release rate for mode I, G_{Ic} (J/m^2)	1270	

Selection of Parameters: General

Calculations have indicated that the SERR in the opening mode is dominant and thus the shear mode is virtually inactive. The critical strain energy release rate as measured by Li (Li, X. et al, 2000) is 1.270N/mm. The next in order of importance is the selection of maximum stress, σ_{max}. This determines the point at which delamination growth initiates. Consider for example the performance of the UEL model (Fig. 4) or the UMAT model (Fig. 6) for various levels of σ_{max}. The most striking feature of the results is that the unloading paths for a given model are parallel to each other; only the crack initiation point - which is almost coincident with the maximum load attained - is different. Thus

crack propagation rate is virtually unaffected by the choice of σ_{max}. Similar observations have been made by the authors elsewhere (Li, Y. et al, 2005 and Alfano, G. et al, 2001).

The following considerations are germane to the selection of the σ_{max}:

(i) The maximum stress must be representative of the tensile strength of the material in which the crack propagates.

(ii) The more physically based cohesive stress-deformation laws involve a rising path till a maximum stress is attained and an unloading path taking the stress to zero when failure is deemed to be complete. On the contrary in the present study the cohesive stress is constant for the most part. If the crack opening displacement is the critical parameter indicating failure, it follows the σ_{max} in our model must be about one half of the actual strength of the material (used in the conventional models).

(iii) At crack initiation, the failure occurs at the crack tip by micro-cracking at an angle into the core as it were. Since we postulate crack growth parallel to the interface, the stress needed to initiate such a crack is probably greater than the actual tensile strength of the material.

The tensile strength of the core material - H200 Divinycell foam - is about 6MPa (Abot, J. L., 2000). The core material is likely to be reinforced due to the presence of a stiff adhesive (of strength 35MPa, Abot, J. L., 2000) bonding the facing sheet with the core for a small distance from the crack interface. It is difficult, therefore to assess precisely the strength of the material; suffice it to say together the effect of the adhesive and the crack kinking at crack initiation (item (iii) above) will put the effective strength significantly more than the actual strength of 6MPa. However in view of item (ii), it is thought appropriate to use the actual strength of 6MPa or values in that range for σ_{max}.

Performance of the UEL model

The finite element model consisted of 4-noded plane strain elements with reduced integration (CPE4R) throughout and the sizes of the element chosen are indicated in Fig. 3. The typical size of the element in the direction of the crack is 0.25mm and thus in one layer there were 840 elements end to end. (A trial run with a coarser mesh with 0.50mm size gave essentially the same results.) Loading was introduced by prescribing the deflection at the point of application of the load and computing the reaction thereof. A total deflection of 30mm was reached in 1000 increments.

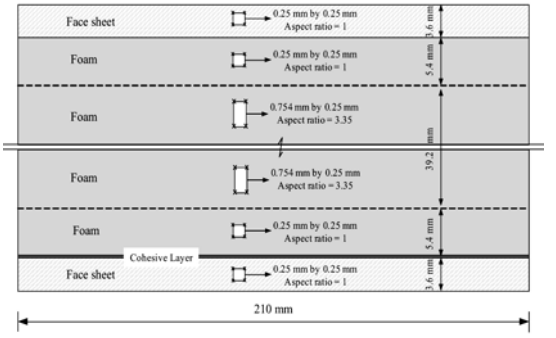

Fig. 3. Finite Element Configuration (not to scale)

The values of the maximum cohesive stress, σ_{max}, selected were 3, 6 and 9MPa respectively. Of these the first and the last are 50% less and 50% more respectively from the nominal strength of the core material, viz. 6MPa. The other parameters of the model: τ_{max} = 20.0Mpa, δ_{10} = 1.e-2, δ_{20} = 1.e-3, G_{Ic} = 1.270N/mm, G_{IIc} is set at an arbitrarily high value.

Li (Li, X., 2000) studied the problem experimentally by a sequence of loading up to incipient crack growth and unloading fully and reloading as before. Fig.4 displays the key points taken from these experimental results which the authors have taken the liberty of re-plotting ensuring the characteristics passed through the origin (elimination of zero error) but maintaining the slopes of the reloading characteristics and the loads recorded at the crack initiation at the end of each loading phase.

As already mentioned, the prediction of crack initiation point depends on the σ_{max} selected – the value of 3MPa is clearly too small for the corresponding behavior is too compliant in the vicinity of crack initiation and a value of 9MPa overestimates the load corresponding to crack initiation. Thus as far as foam core sandwich members are concerned , we may conclude that reasonable results can be obtained by selecting for σ_{max} the actual strength of the core for delamination predictions using the UEL model. A typical stress distribution around the crack tip is shown in Fig. 5 where it is seen that the model preserves the features of a sharp crack with a highly localized stress concentration with little damage upstream of the crack.

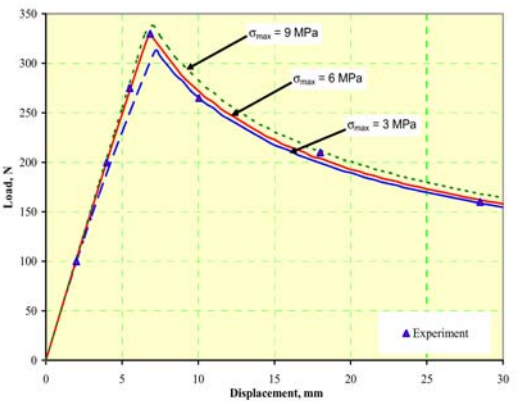

Fig. 4. Simulation results from UEL model vs. experimental results

Performance of the UMAT model

The finite element mesh configuration selected for the analysis is similar to the one used for the UEL model except for the mesh size in the longitudinal direction which is now 0.5mm. Two values of strength were investigated, viz. 7MPa and 9.4MPa which are marginally higher than those used for the UEL model. It was anticipated that the strength needed for the UMAT model must be higher than that employed for the UEL model, to compensate for the influence of compressive stress developing in the cohesive layer upstream of the crack. However, the analysis revealed that the cohesive zone (that part of the cohesive layer which is in tension starting from the crack tip) was sufficiently long (12 elements in length) so that this effect is not significant.

The results obtained for the two values of σ_{max} exhibit the same trend (Fig. 6), but differ in their prediction of crack initiation as seen in the UEL model results. The crack initiation results agree well with UEL model results obtained with comparable values of σ_{max} (Fig. 7). However there is an obvious and a significant difference between the UMAT results and UEL results which is highlighted in Fig. 7. It is seen that the UMAT model predicts that the crack ceases to grow after some growth and the load then begins to gradually increase with the crack opening displacement. There is no reason to suppose that such a prediction has any validity to it and in fact can be shown to be due to an intrinsic deficiency of the model.

Fig. 7 illustrates what happens when an initial crack length l_o higher than 51mm is assumed, say 71mm. The load-displacement characteristic has a smaller slope and crack initiation occurs at a point which lies on or close to the unloading characteristic associated with lo = 51mm. But the unloading characteristic associated with l_o = 71mm deviates from that associated with an initial crack length of 51mm and lies closer to that given by the experiment and UEL model. However this characteristic too gradually deviates from the correct result. It is clear therefore that the UMAT model, though capable of predicting crack initiation correctly gradually loses its ability to predict continued crack growth.

Fig. 8 shows the magnified image of stress distribution in the close vicinity of the crack tip when the crack opening displacement measured at the point of load application is 25mm, At this instant crack has progressed to a length of 101mm and the next crack tip element is on the point of failure.

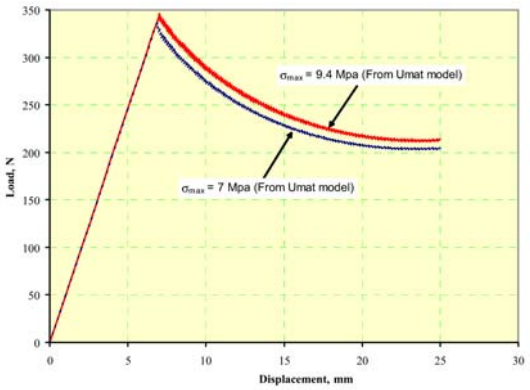

Fig. 6. Simulation results from UMAT model

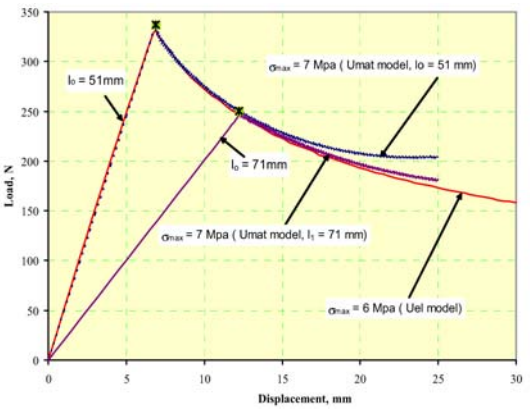

Fig. 7. Comparison between UEL results and UMAT results

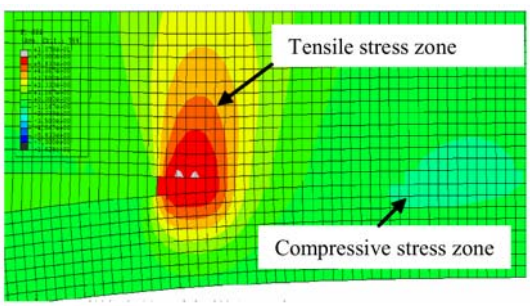

Fig. 8. Stress distribution around crack tip

Fig. 9 shows the magnified view of the deformation of the bottom surface of the cohesive elements close to the crack tip for the two cases: (i) The current crack length (l_{cr}) of 101mm is reached after a crack extension of 50mm from the initial crack length (l_o) of 51mm, and (ii) The initial crack length is taken as 101mm and the crack tip element is on the verge of failure ($l_{cr} = l_o$ = 101mm). Note that the downward deflections are plotted above the x-axis in the figure.

There are two features that may be observed in these pictures:

(i) From Fig 8 , it is seen that there is a part of cohesive layer which carries tensile stress in the vicinity of the crack tip, but more significantly this stress gradually diminishes to zero as we travel upstream of the crack and changes to compression.

(ii) In case (i) the depth of the cohesive layer reduces as we travel upstream from the crack tip and a "neck" – a region of slightly reduced depth compared to neighboring regions on either side appears. The bottom surface of the cohesive elements is undulating at the crack tip. This is in contrast to the case (ii) which exhibits a smooth variation of the cohesive layer.

It is clear that item (ii) must be a result of what transpires during the failure of cohesive elements and the accompanying crack extension. As each element fails certain force is released on to the delaminated sheet which rotates so as to compress the cohesive layer downstream. Once a "neck" of certain threshold acuteness is formed, the crack growth is at first seriously inhibited and eventually stops.

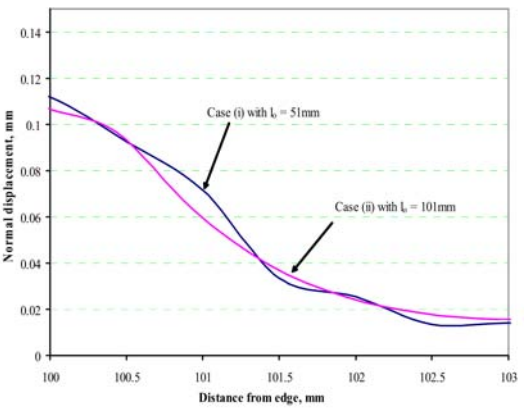

Fig. 9. Displacements along the bottom surface of the cohesive elements (when σ_{max} = 7Mpa)

These phenomena are fairly insignificant or virtually absent in the UEL model. Of these, item (i) can have an effect on crack initiation as the compression block upstream can send a wave of transverse compressive stress towards the crack tip thereby delaying the crack initiation. However, as already mentioned this effect appears to be not significant for sandwich members as the cohesive zone is of greater length than in laminated composites – of the order of 6-7mm. The second factor, too, kicks in much later, so much so the UMAT model can be used for a study of delamination in sandwich beams if one is not investigating large crack extensions.

Response of sandwich columns under compression

In this section we study the response of a compressed column. The compression carried by the column is small relative to the buckling load of the column. We note that the corresponding static problem has been studied by El-Sayed, S. et al, 2002 using a variant of the UMAT model which incorporates an unloading phase of the cohesive material response. The present study uses the UEL model for the problem and the salient features of the static response are briefly summarized. Two cases are considered; the first one is that of a relatively stout column with relatively thick facing sheets and the second is that of a slender column having very thin facing sheets.

Case I

Geometry, Materials and Boundary Conditions

The core and facing materials are exactly the same as the test specimen (Table 1) discussed in the last section and the cross-section of the member investigated is also the same (h = 50mm, t = 3.6mm). The total length of the column investigated is 420mm and it is considered clamped at either end. Because of symmetry involved – barring the unlikely scenario of sudden interference of antisymmetric modes of bifurcation- only half the column length of 210mm included between the line of symmetry on the left and the clamped end on the right is considered (Fig. 10). A rigid surface incapable of rotation and lateral translation is created to model the clamped end. A symmetrically located initial delamination of

total length 102mm is deemed to exist between bottom facing sheet and the core. Fig. 10 shows the configuration and other pertinent details.

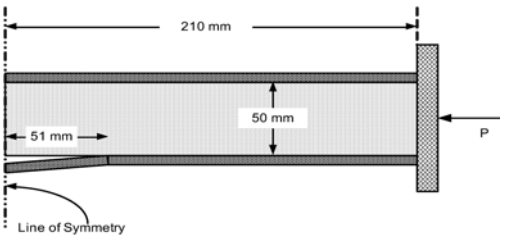

Fig. 10. Configuration of case I

Details of the Analysis

Finite Element mesh configuration is the same as in Fig. 3 though the length of the column and the cohesive layer elements are different. The size of the elements is 0.25mm in the longitudinal direction and plane strain elements (CPE4R) with reduced integration were employed in the analysis as before. Unlike the previous example, the column is treated as having unit width (1mm) and the loads are reported as per unit width. The load is inducted by prescribing the end-shortening (relative to the plane of symmetry). The critical value of SERR in the opening mode is once again taken as 1.27N/mm. The value of maximum stress, σ_{max} is taken as 10MPa and δo is taken as before equal to 0.01mm.

The model was perturbed slightly by incorporating imperfections in order to keep the delamination open and prompt the structure towards delamination buckling and growth. To this end, a linear stability analysis without the cohesive layer was conducted and the buckling loads and modes were obtained. The first three buckling loads were found to be 562N, 2079N and 3466N respectively. Of these the first (Fig. 11(a)) and the second (Fig. 11(b)) pertain to delamination buckling – the former keeps the delamination fully open and the latter partially closed. The last one (Fig. 11(c)) is an overall buckling mode. It is clear that the first alone is critical and therefore an imperfection in the form of this mode is incorporated in the model with a maximum deflection of 0.5mm at the center. Given the stoutness of the member (relative to the length, L/d =7.3) and the magnitude of the overall buckling load, it is clear that overall bending of the column plays a relatively minor role in the problem.

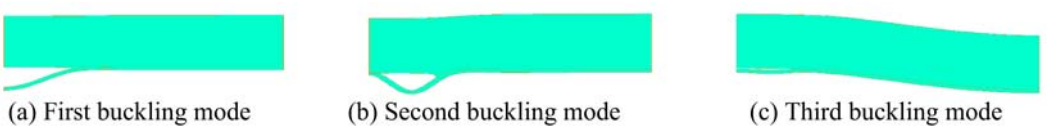

Fig. 11. The first three buckling modes

Buckling and Delamination

The column is compressed in a quasi-static manner, so that end-shortening increases from zero to a value at which the facings undergo an average strain of 1.5%. Nonlinearity sets in as soon as the delamination tends to buckle outward and at a load of 650N/mm (a longitudinal stress of 116MPa in the facing sheets) delamination begins to grow (Fig. 12). At first this is rather rapid and occurs with little increase in load (points A, B and C in Fig. 12), but soon settles down to a relatively modest rate and delamination occurs under increasing load thereafter. Finally at load of 1380N/mm (average stress of 246MPa), a limit point is reached and thereafter delamination growth is accompanied by shedding of the load by the member. At a load of 1294N/mm the delamination length recorded is 152.25 (the end-shortening = 3.15mm). Compressed to an end-shortening of say 3.5mm, almost complete delamination of the bottom facing occurs, but this would necessarily be accompanied by other forms of failure not considered here. Fig. 12 shows the variation of the load with end-shortening. The observed behavior is in very good agreement to that obtained by EL-Sayed, S., 2002 (not shown) though their model tends to be slightly stiffer at the more advanced delamination range. Also indicated in the figure are the delamination growths recorded at certain significant points in the history - in

particular the values corresponding to end -shortening magnitudes of 0.8mm, 1.0mm and 1.2mm respectively. Fig. 13 shows the deformed shape when end shortening is 2mm.

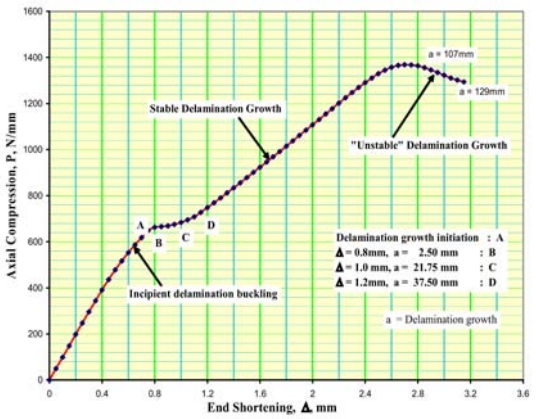

Fig. 12. Response of sandwich column under static loading, Case I

Fig. 13. Static response for case I: Deformed shape at an end shortening of 2mm

Case II

We next consider a sandwich column (Fig. 14) which is significantly slender in comparison to that presented in Case I. The column is clamped at its ends as before, the total length (L) now is 300mm and the total depth, d is 20mm. Thus the L/d is twice that in Case I. Further the thickness of the facing sheets, t is only 0.5mm each and thus d/t = 40 – again about thrice as much as in Case I. The motivation for studying such a case is to examine the influence of overall bending and wrinkling on the delamination growth. (The geometry is the same as that studied by El-Sayed, S., 2002). An initial delamination of the top facing sheet of 10mm at the center was considered (5mm on either side of symmetry).

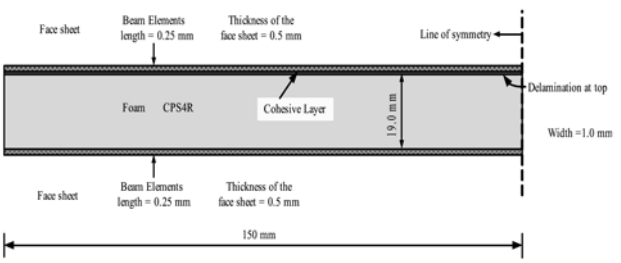

Fig. 14. Configuration of slender sandwich beam

Both the core and facing sheets are assumed to be isotropic, for simplicity with: $E_f = 26900$MPa, $\nu_f = 0.3$ and $E_c = 269$MPa, $\nu_c = 0.3$, where E and ν stand respectively for Young's modulus and Poisson ratio and the subscripts f and c stand for the facings and the core respectively. Two values of G_{Ic} are considered, viz. 1.270N/mm^2 and 0.635N/mm^2, with $\sigma_{max} = 6$MPa and $\delta_o = 0.01$mm.

Finite Element Modeling

In view of the relatively small thickness of the facing sheets, modeling it with solid elements was not considered viable as the aspect ratio of the four noded elements needs to be maintained around unity. Therefore it was decided to use 2-noded shear-deformable beam elements to model the facing sheets. The core was modeled using 4-noded plane stress elements (CPS4R) with reduced integration.

The reference nodes of the beam elements of the top sheet were placed at the bottom of the beam section and those of the bottom sheet at the top of the section in order to ensure deformation compatibility with core elements. The element size along the longitudinal direction was maintained at 0.25mm and thus there were 600 elements in each layer of elements. The aspect ratios of the core elements were kept around unity. The width of the column was taken as 1mm as before.

Details of Static Nonlinear Analysis

As before, a linear stability analysis was performed to find the critical loads at which significant deformation will appear. The critical loads associated with delamination buckling and overall buckling were found to be 157.6N and 721.0N respectively. It will be seen as delamination buckling and growth occur the effective center of stiffness moves downwards and as a result some overall bending occurs at a fraction of the critical load associated with overall buckling predicted by linear stability analysis. This is clearly an example of interaction of delamination growth and overall buckling.

Load was introduced by prescribing end-shortening as before. The maximum end-shortening of 2mm is selected which is about 2.5 times that corresponding to delamination buckling. Small equal and opposite loads increasing from zero to 1N were applied at the bottom and top nodes respectively at the center of the column to prompt the delamination to remain open. End-shortening was applied in small increments, 1000 increments to reach a value of 2mm.

Features of Nonlinear Response

Consider first the case with G_{Ic} = 1.27N/mm. As the end-shortening increases to beyond the critical value, delamination occurs with about 12 elements (each 0.25mm long) failing one after another in quick succession. The load drops slightly but thereafter recovers to increase further. During this stage more elements fail with a total delamination growth of 9mm when the end-shortening of 2mm is reached. At this time the tangential stiffness of the structure has reduced significantly with the load beginning to level off. The behavior for G_{Ic} = 0.637N/mm is similar, except that delamination growth begins a little early, the load drop is more pronounced. And the total delamination growth is 18mm. Fig. 15 shows the axial compression vs. end shortening relationship.

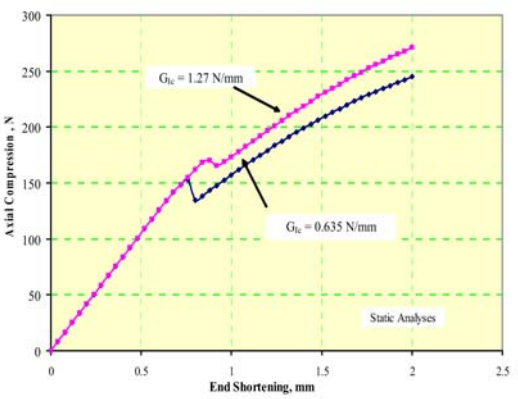

Fig. 15. Static Response of Sandwich Column, Case II

Notwithstanding the actual magnitudes of the loads involved, qualitatively there is a significant difference between the delamination behavior under static loading of the Cases I and II considered here (cf. Fig. 13 and Fig. 16). It is somewhat paradoxical to see that delamination growth is minimal for the present case of a slender column with thin facing sheets whereas it was extensive for the case of stouter column with thicker facing sheets. Careful examination of the deformed shape of the member as it evolves indicates that the delamination growth is influenced by overall bending of the entire column and highly localized rotation of the facing sheet that occurs at the crack tip. If the overall bending is such as to cause longitudinal tension at the facing sheet, delamination growth comes to a stand still; if it is such as to cause longitudinal compression in the delaminating facing sheet with

a pronounced curvature, the sheet in the vicinity of the crack tip tends to rotate and come into contact with the core inhibiting delamination growth. Thus we may conclude the delamination growth is not a significant factor in a slender sandwich column having thin facings under static loading. There are other modes of failure, such as face sheet wrinkling and its interaction with overall bending which cause failure of the member (El-Sayed, S., 2002).

Fig. 16. Static Response, Case II: Deformed shape at end shortening = 2mm

Conclusions

The delamination phenomena in sandwich members are studied using cohesive layer models-designated as UMAT and UEL models. When applied to a test case, it was found that the UMAT model which has a finite thickness can predict initiation of delamination growth as well as rate of growth of delamination, but is unable to predict large delamination growth due to an inherent deficiency. The UEL model which has zero initial thickness is capable of tracing the entire delamination history. Apart from the critical value of strain energy release rate in the opening mode, the parameter that influences crack initiation is the strength of the cohesive model material; for sandwich delamination problems using the actual strength of the core material in conjunction with the proposed models gave satisfactory results.

Delamination was studied in a member carrying a prescribed end-shortening. Two cases are considered, the Case I of a column which was relatively stout with relatively thick facing sheets and Case II, a slender column with thin facing sheets. The overall bending of the member (in case II) had a significant influence in inhibiting the crack growth by virtue of contact between the facing sheet and the core in the quasi-static load application.

References

ABAQUS/Standard User's Manual, "UMAT: Define a Material's Mechanical Behavior," Hibbitt, Karlsson and Sorensen, Inc., Pawtucket, RI, Vol. 6.3, 2001, pp. 24.2.30.1-24.2.30.14.

ABAQUS/Standard User's Manual, "UEL: Define an Element," Hibbitt, Karlsson and Sorensen, Inc., Pawtucket, RI, Vol. 6.3, 2001, pp. 24.2.19.1-24.2.19.17.

Abot, J. L., "Fabrication, Testing and Analysis of Composite Sandwich Beams", Ph.D. Thesis, Northwestern University, Evanston, Illinois, 2000.

Alfano, G. and Crisfield, M. A., "Finite Element Interface Models for the Delamination Analysis of Laminated Composites: Mechanical and Computational Issues," *International Journal for Numerical Methods in Engineering*, Vol. 50, 2001, pp. 1701-1736.

El-Sayed, S. and Sridharan, S., "Cohesive Layer Models for Predicting Delamination Growth and Crack Kinking in Sandwich Structures," *International Journal of Fracture,* Vol. 117, No. 1, Sept. 2002, pp. 63-84.

Li, X., "Debonding fracture of foam core the tilted sandwich structure," Ph.D. Thesis, Florida Atlantic University, Boca Raton, Florida, 2000.

Li, Y. and Sridharan, S., "Performance of Two Distinct Cohesive Layer Models for Tracking Composite Delamination", International Journal of Fracture, in press, 2005.

Li, Y. and Sridharan, S., "Investigation of Delamination Caused by Impact Using a Cohesive Layer Model", AIAA Journal, Vol.43,No.10,2005, pp.2243-2250.

Sridharan, S., "Displacement-based mode separation of strain energy release rates for interfacial cracks in bi-material media", International Journal of Solids and Structures, Vol. 38, 2001, pp. 2787-6803.